Acta Cryst E CRYSTALLOGRAPHIC COMMUNICATIONS
ISSN 2056-9890

trans-Dichloridobis(dimethyl sulfoxide-κO)bis(4-fluorobenzyl-κC^1)tin(IV): crystal structure and Hirshfeld surface analysis

Nur Adibah Binti Mohd Amin,[a] Rusnah Syahila Duali Hussen,[a] See Mun Lee,[b] Nathan R. Halcovitch,[c] Mukesh M. Jotani[d]‡ and Edward R. T. Tiekink[b]*

[a]Department of Chemistry, University of Malaya, 50603 Kuala Lumpur, Malaysia, [b]Research Centre for Crystalline Materials, School of Science and Technology, Sunway University, 47500 Bandar Sunway, Selangor Darul Ehsan, Malaysia, [c]Department of Chemistry, Lancaster University, Lancaster LA1 4YB, United Kingdom, and [d]Department of Physics, Bhavan's Sheth R. A. College of Science, Ahmedabad, Gujarat 380001, India. *Correspondence e-mail: edwardt@sunway.edu.my

Received 30 March 2017
Accepted 2 April 2017

Edited by M. Weil, Vienna University of Technology, Austria

‡ Additional correspondence author, e-mail: mmjotani@rediffmail.com.

Keywords: crystal structure; organotin; C—H···F interactions; Hirshfeld surface analysis.

CCDC reference: 1541712

Supporting information: this article has supporting information at journals.iucr.org/e

The Sn^{IV} atom in the title diorganotin compound, $[Sn(C_7H_6F)_2Cl_2(C_2H_6OS)_2]$, is located on a centre of inversion, resulting in the $C_2Cl_2O_2$ donor set having an all-*trans* disposition of like atoms. The coordination geometry approximates an octahedron. The crystal features C—H···F, C—H···Cl and C—H···π interactions, giving rise to a three-dimensional network. The respective influences of the Cl···H/H···Cl and F···H/H···F contacts to the molecular packing are clearly evident from the analysis of the Hirshfeld surface.

1. Chemical context

The structural chemistry of organotin(IV) compounds with multidentate Schiff base ligands has been of interest since the observation of the diversity in their supramolecular association patterns (Teoh *et al.*, 1997; Dey *et al.*, 1999). Typically, these multidentate ligands bind to the tin atom through the phenolic-O, imine-N, oxime-O or even oxime-N atoms. In view of this, the coordination of these multidentate ligands to (organo)tin may lead to more thermodynamically stable organotin complexes, in contrast to those with monodentate ligands (Vallet *et al.*, 2003; Contreras *et al.*, 2009), a feature which could potentially be useful in catalytic studies (Yearwood *et al.*, 2002). In consideration of this and as part of ongoing work with multidentate ligands of organotin compounds (Lee *et al.*, 2004), an attempt to synthesize an adduct of the potentially tetradentate Schiff base *N,N*-1,1,2,2-dinitrilevinylene*bis*(5-bromosalicylaldiminato) with di(*p*-fluorobenzyl)tin(IV) dichloride was made.

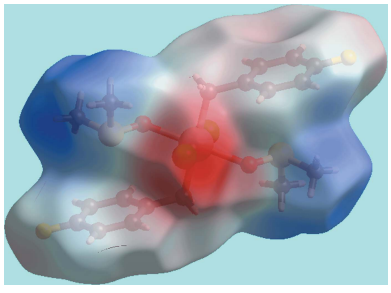

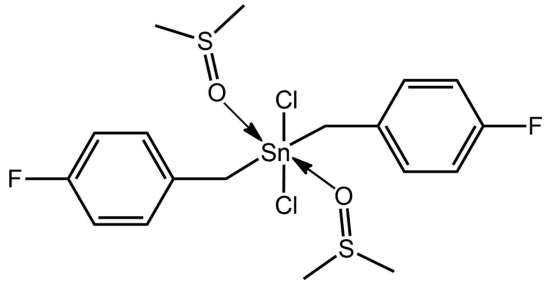

The complex was obtained as an orange powder and was successfully characterized using various spectroscopic methods including ^{1}H NMR spectroscopy. Upon interaction with DMSO-d_6, in the context of NMR studies, colourless

Table 1
Selected geometric parameters (Å, °).

Sn—C1	2.1628 (16)	Sn—Cl1	2.5599 (4)
Sn—O1	2.2332 (11)		
C1—Sn—O1	95.99 (5)	C1—Sn—Cl1^{i}	89.95 (5)
C1—Sn—Cl1	90.05 (5)	O1—Sn—Cl1	90.44 (3)
C1—Sn—O1^{i}	84.01 (5)	O1—Sn—Cl1^{i}	89.56 (3)

Symmetry code: (i) $-x+1, -y+1, -z+1$.

crystals were obtained after several weeks standing. The formation of the new title compound, (I), is likely due to degradation of the complex while stored in the NMR tube. In the present contribution, the crystal and molecular structures of (I) are described as well as a detailed analysis of the intermolecular association through a Hirshfeld surface analysis.

2. Structural commentary

The molecular structure of (I), Fig. 1, has the Sn^{IV} atom situated on a crystallographic centre of inversion. The Sn^{IV} atom is coordinated by monodentate ligands, *i.e.* chloride, sulfoxide-O and methylene-C atoms. From symmetry, each donor is *trans* to a like atom resulting in an all-*trans*-$C_2Cl_2O_2$ donor set about the Sn^{IV} atom. The donor set defines a distorted octahedral geometry owing, in part, to the disparate Sn—donor atom bond lengths, Table 1. The angles about the Sn^{IV} atom differ relatively little from the ideal octahedral angles with the maximum deviation of *ca* 6° noted for the C1—Sn—O1 angle, Table 1.

3. Supramolecular features

The molecular packing in (I) comprises C—H···F, C—H···Cl and C—H···π interactions which combine to generate a three-dimensional network, Table 2. The chloride atom participates in phenyl-C6—H···Cl1 and methyl-C8—H···Cl1 interactions. As each chloride atom is involved in two C—H···Cl interactions and there are two chloride atoms per molecule, the C—H···Cl interactions extend laterally to give rise to a supramolecular layer in the *bc* plane, Fig. 2*a*. Layers are connected along the *a* axis by phenyl-C3—H···F1 and methyl-C9—H···π(phenyl) interactions to consolidate the molecular packing, Fig. 2*b*.

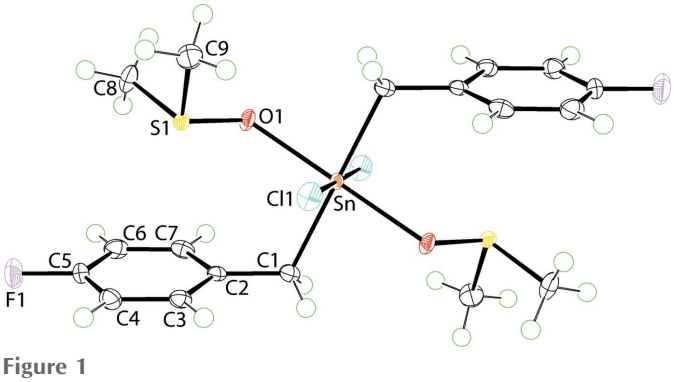

Figure 1
The molecular structure of (I), showing the atom-labelling scheme and displacement ellipsoids at the 70% probability level. The Sn^{IV} atom lies on a centre of inversion; unlabelled atoms are related by the symmetry operation $1-x, 1-y, 1-z$.

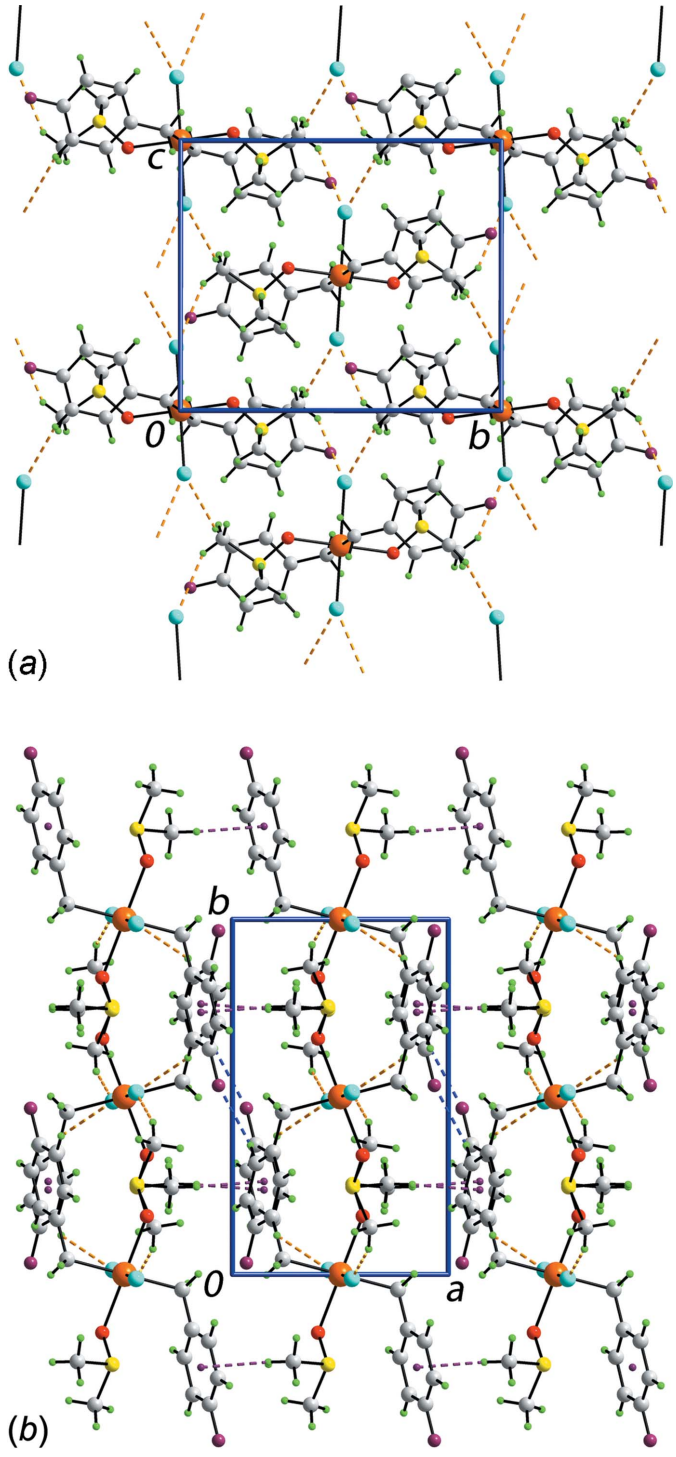

Figure 2
The molecular packing in (I): (*a*) supramolecular layer in the *bc* plane sustained by C—H···Cl interactions and (*b*) a view of the unit-cell contents in projection down the *c* axis. The C—H···Cl, C—H···F and C—H···π interactions are shown as orange, blue and purple dashed lines, respectively.

Table 2
Hydrogen-bond geometry (Å, °).

*Cg*1 is the centroid of the C2–C7 ring.

D—H···*A*	*D*—H	H···*A*	*D*···*A*	*D*—H···*A*
C3—H3···F1^{ii}	0.95	2.49	3.333 (2)	147
C6—H6···Cl1^{iii}	0.95	2.77	3.6129 (18)	148
C8—H8*B*···Cl1^{iv}	0.98	2.76	3.6379 (17)	150
C9—H9*C*···*Cg*1^{v}	0.98	2.67	3.3887 (19)	130

Symmetry codes: (ii) $-x, y+\frac{1}{2}, -z+\frac{1}{2}$; (iii) $x, -y-\frac{1}{2}, z-\frac{1}{2}$; (iv) $-x+1, y-\frac{1}{2}, -z+\frac{1}{2}$; (v) $x+1, y, z$.

4. Hirshfeld surface analysis

The Hirshfeld surface analysis on the structure of (I) provides more insight into the molecular packing and was performed as described recently (Wardell *et al.*, 2016). It is evident from the bright-red spots appearing near the chloride and fluoride atoms on the Hirshfeld surface mapped over d_{norm} in Fig. 3 that these atoms play a significant role in the molecular packing. Thus, the bright-red spots near phenyl-H6, methyl-H8*B* and a pair near Cl1 in Fig. 3 indicate the presence of bifurcated C—H···Cl interactions formed by each of the chloride atoms. Similarly, the pair of red spots near phenyl-H3 and F1 atoms are associated with the donor and acceptor of C—H···F interactions, respectively. The donors and acceptors of C—H···Cl and C—H···F interactions are also represented with blue (positive potential) and red regions (negative potential), respectively, on the Hirshfeld surface mapped over the electrostatic potential in Fig. 4. In addition to above, the Cl1 and F1 atoms also participate in short interatomic contacts with methyl-H atoms, Table 3. The presence of faint-red spots near the phenyl-C4 and methyl-C9 atoms in Fig. 3 indicate their participation in a short interatomic C···C contact, Table 3, which compliments the methyl-C—H···π(phenyl) contact described above. The presence of the C—H···π interaction is also evident from the view of Hirshfeld surface mapped over the electrostatic potential around participating atoms, Fig. 4; the donors and acceptors of these interactions are viewed as the convex surface around atoms of the methyl-C9 groups and the concave surface above the (C2–C7) phenyl ring, respectively. The immediate environments about a reference molecule within d_{norm}- and shape-index-mapped Hirshfeld surfaces highlighting the various C—H···Cl, C—H···F and C—H···π interactions are illustrated in Fig. 5*a–c*, respectively.

The overall two-dimensional fingerprint plot and those delineated into H···H, Cl···H/H···Cl, F···H/H···F, C···H/H···C and O···H/H···O contacts (McKinnon *et al.*, 2007) are illustrated in Fig. 6*a–f*, respectively, and their relative contributions to the Hirshfeld surfaces are summarized in Table 4. It is clear from the fingerprint plot delineated into H···H contacts, Fig. 6*b*, that although these contacts have the greatest contribution, *i.e.* 45.7%, to the Hirshfeld surface, the disper-

Table 3
Summary of short interatomic contacts (Å) in (I).

Contact	distance	symmetry operation
C4···C9	3.371 (2)	$-1+x, y, z$
F1···H8*A*	2.66	$1-x, -y, 1-z$
Cl1···H9*B*	2.91	$1-x, \frac{1}{2}+y, \frac{1}{2}-z$

Note: (*a*) the Sn^{IV} atom is located on a centre of inversion.

Table 4
Percentage contribution of interatomic contacts to the Hirshfeld surface for (I).

Contact	percentage contribution
H···H	45.7
Cl···H/H···Cl	15.1
F···H/H···F	19.8
C···H/H···C	12.8
O···H/H···O	4.1
S···H/H···S	1.7
Cl···F/F···Cl	0.6
C···Cl/Cl···C	0.1
F···F	0.1

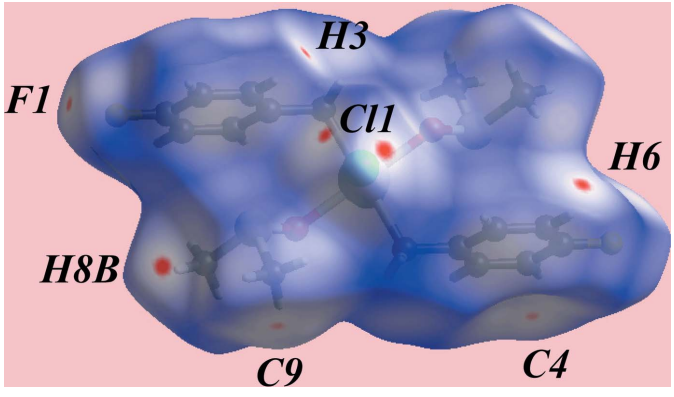

Figure 3
A view of the Hirshfeld surface for (I) mapped over d_{norm} over the range −0.049 to 1.356 au.

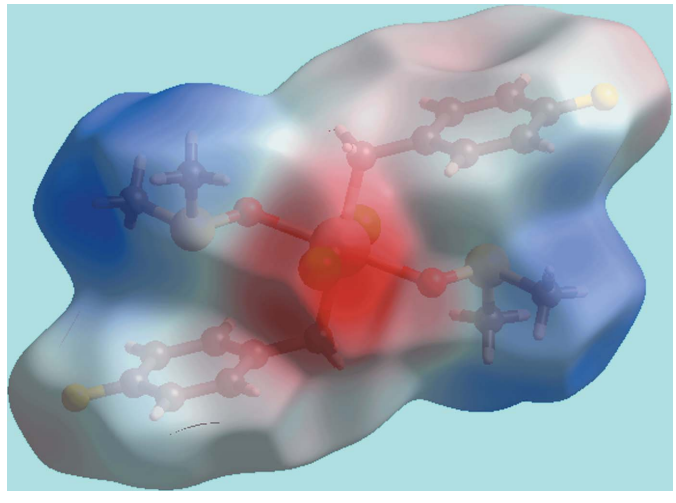

Figure 4
A view of the Hirshfeld surface for (I) mapped over the electrostatic potential in the range ±0.095 au.

sion forces acting between them keep these atoms at the distances greater than the sum of their van der Waals radii, hence they do not contribute significantly to the molecular packing. The comparatively greater contribution of F···H/H···F contacts to the Hirshfeld surface *cf.* Cl···H/H···Cl contacts, Table 4, is due to the relative positions of the chloride and fluoride atoms in the molecule, the fluoride atoms being at the extremities and the chloride atoms near the tin(IV) atom. However, the Cl···H/H···Cl contacts have a greater influence on the molecular packing as viewed from the delineated fingerprint plot in Fig. 6*c*. The forceps-like distribution of points in the plot with tips at $d_e + d_i \sim 2.8$ Å result from the bifurcated C—H···Cl interactions, and points at positions less than the sum of their van der Waals radii are ascribed to the short interatomic Cl···H/H···Cl contacts, the green appearance due to high density of interactions. Similarly, a pair of short spikes at $d_e + d_i \sim 2.5$ Å in the fingerprint plot delineated into F···H/H···F contacts, Fig. 6*d*, are indicative of intermolecular C—H···F interactions with the short interatomic F···H/H···F contacts merged within the fingerprint plot. It is important to note from the fingerprint plot delineated into C···H/H···C contacts, Fig. 6*e*, that even though their interatomic distances are equal to or greater than the sum of their van der Waals radii, *i.e.* 2.9 Å, the 12.8% contribution from these to the Hirshfeld surfaces are indicative of the presence of C—H···π interactions in the structure. This is also justified from the presence of short interatomic C···C contacts, Fig. 5*c* and Table 3. The 4.1% contribution from O···H/H···O contributions to Hirshfeld surfaces, Fig. 6*f*, and the small

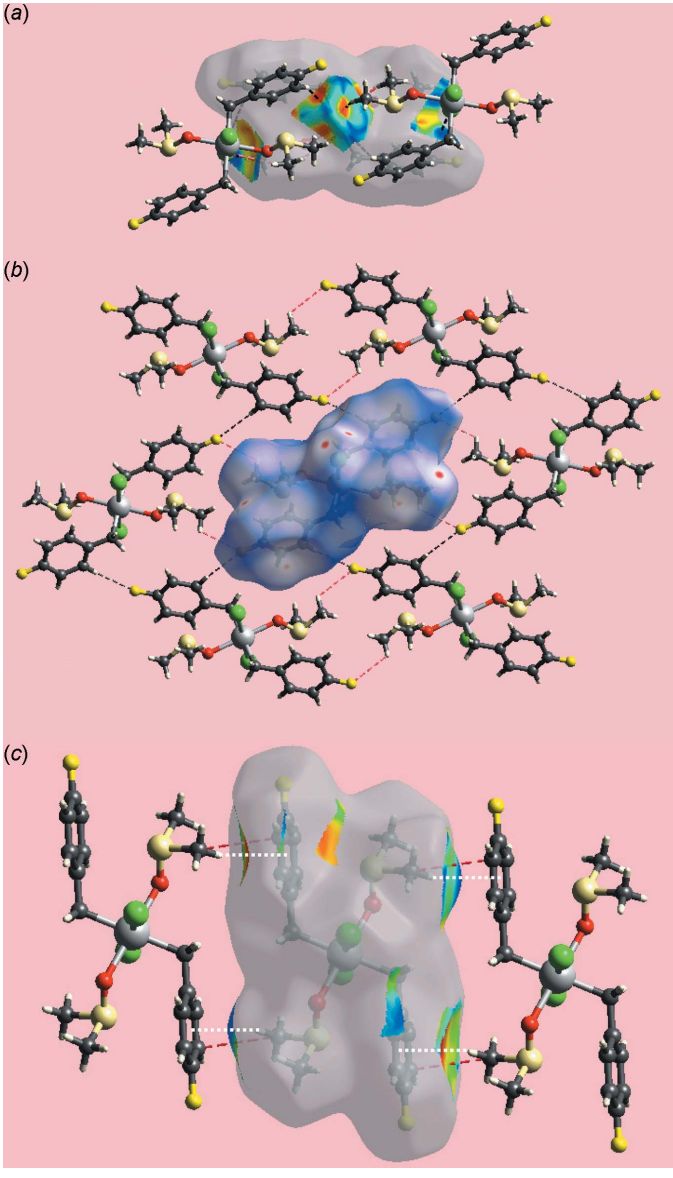

Figure 5
Views of the Hirshfeld surfaces about a reference molecule mapped over (*a*) shape-index, (*b*) d_{norm} and (*c*) shape-index, highlighting (*a*) C—H···F and short interatomic F···H/H···F contacts as black and red dashed lines, respectively, (*b*) C—H···Cl and short interatomic Cl···H/H···Cl contacts as black and red dashed lines, respectively, and (*c*) C—H···π and short interatomic C···C contacts as white and red dashed lines, respectively.

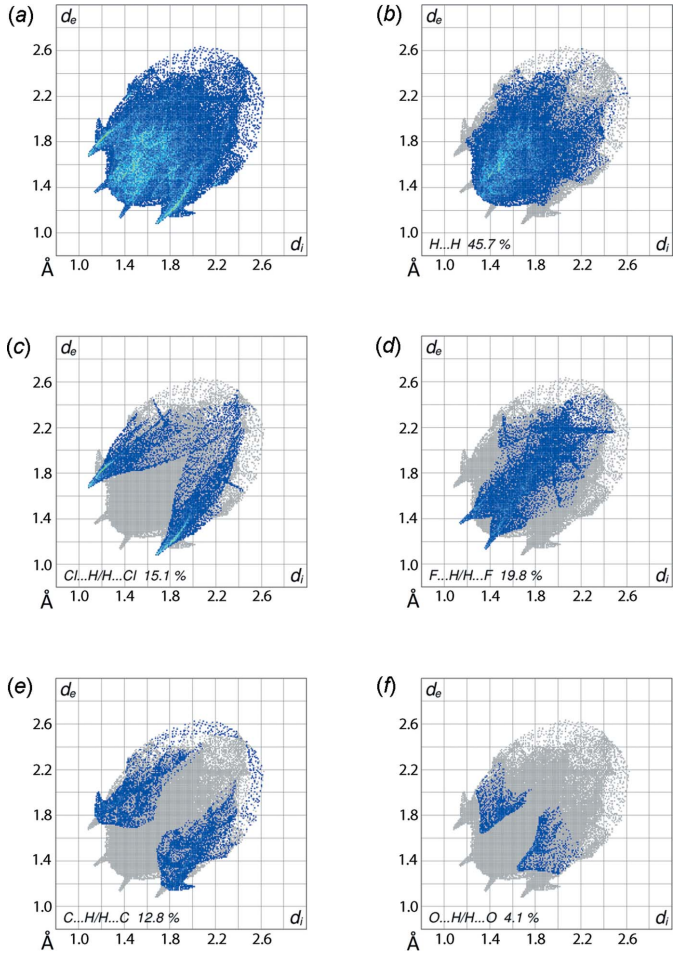

Figure 6
Fingerprint plots for (I): (*a*) overall and those delineated into (*b*) H···H, (*c*) Cl···H/H···Cl, (*d*) F···H/H···F, (*e*) C···H/H···C and (*f*) O···H/H···O contacts.

Table 5
Selected geometric parameters (Å, °) for molecules of the general formula $R_2SnX_2(DMSO)_2$.

Compound	X—Sn—X	O—Sn—O	C—Sn—C	Reference
$Me_2SnBr_2(DMSO)_2$	180	180	180	Aslanov *et al.* (1978)
$Me_2SnCl_2(DMSO)_2$	95.2 (3)	83.7 (5)	172.7 (3)	Aslanov *et al.* (1978)
$Ph_2SnCl_2(DMSO)_2$	97.43 (3)	79.34 (9)	172.17 (14)	Sadiq-ur-Rehman *et al.* (2007)
$(4\text{-}FC_6H_4CH_2)_2SnCl_2(DMSO)_2$	180	180	180	This work

contributions from the other contacts listed in Table 2 have a negligible effect on the packing.

5. Database survey

There are three related structures of the general formula $R_2SnX_2(DMSO)_2$ in the crystallographic literature (Groom *et al.*, 2016). Key bond angles for these are listed in Table 5. The $Me_2SnBr_2(DMSO)_2$ compound (Aslanov *et al.*, 1978) is analogous to (I) in that the Sn^{IV} atom is located on a centre of inversion and hence, is an all-*trans* isomer. The two remaining structures have a different arrangements of donor atoms with the common feature being the *trans*-disposition of the Sn-bound organic groups, with the halides and DMSO-O atoms being mutually *cis*, i.e. R = Me and X = Cl (Aslanov *et al.*, 1978; Isaacs & Kennard, 1970) and R = Ph and X = Cl (Sadiq-ur-Rehman *et al.*, 2007). Clearly, further studies are required to ascertain the factor(s) determining the adoption of one coordination geometry over another.

6. Synthesis and crystallization

All chemicals and solvents were used as purchased without purification. Di(*p*-fluorobenzyl)tin dichloride was prepared in accordance with the literature method (Sisido *et al.*, 1961). All reactions were carried out under ambient conditions. The melting point was determined using an Electrothermal digital melting point apparatus and was uncorrected. The IR spectrum was obtained on a Perkin Elmer Spectrum 400 FT Mid-IR/Far-IR spectrophotometer in the range 4000 to 400 cm^{-1}. The ^1H NMR spectrum was recorded at room temperature in $CDCl_3$ solution on a Jeol ECA 400 MHz FT–NMR spectrometer.

N,*N*′-1,1,2,2-Dinitrilevinylenebis(5-bromosalicylaldiminato) (1.0 mmol, 0.401 g; prepared by the condensation reaction between diaminomaleonitrile and 5-bromosalicylaldehyde in a 2:1 molar ratio in ethanol) and triethylamine (1.0 mmol, 0.14 ml) in ethyl acetate (25 ml) was added to di(*p*-fluorobenzyl)tin dichloride (1.0 mmol, 0.183 g) in ethyl acetate (10 ml). The resulting mixture was stirred and refluxed for 4 h. The filtrate was evaporated until a dark-orange precipitate was obtained. The precipitate was dissolved in DMSO-d_6 solution in a NMR tube for ^1H NMR spectroscopic characterization. After the analysis, the tube was set aside for a month and colourless crystals of (I) suitable for X-ray crystallographic studies were obtained from the slow evaporation. Yield: 0.060 g, 11%; m.p: 399 K. IR (cm^{-1}): 1595(m) ν(C═C), 1504(s) ν(S═O), 1161(*m*), 578(*w*), 508(*m*) ν(Sn—O). ^1H NMR (in $CDCl_3$): 6.90–7.11, 7.35–7.40 (*m*, 8H, aromatic-H), 3.11 (*s*, 6H, –CH_3), 2.17 (*m*, 4H, –CH_2).

7. Refinement details

Crystal data, data collection and structure refinement details are summarized in Table 6. Carbon-bound H-atoms were placed in calculated positions (C—H = 0.95–0.99 Å) and were included in the refinement in the riding model approximation, with U_{iso}(H) set to 1.2–1.5U_{eq}(C).

Funding information

Funding for this research was provided by: Sunway University (award No. INT-RRO-2017–096); University of Malaya (award Nos. RP017A-2014AFR, PG239–2016\#65532;A); Ministry of Higher Education, Malaysia (MOHE) Fundamental Research Grant Scheme (award No. FP033–2014B).

Table 6
Experimental details.

Crystal data	
Chemical formula	$[Sn(C_7H_6F)_2Cl_2(C_2H_6OS)_2]$
M_r	564.08
Crystal system, space group	Monoclinic, $P2_1/c$
Temperature (K)	100
a, b, c (Å)	8.2363 (1), 12.7020 (2), 11.4038 (1)
β (°)	110.391 (2)
V (Å^3)	1118.28 (3)
Z	2
Radiation type	Cu $K\alpha$
μ (mm^{-1})	13.28
Crystal size (mm)	0.24 × 0.12 × 0.10
Data collection	
Diffractometer	Agilent SuperNova, Dual, Cu at zero, AtlasS2
Absorption correction	Multi-scan (*CrysAlis PRO*; Rigaku Oxford Diffraction, 2015)
T_{min}, T_{max}	0.636, 1.000
No. of measured, independent and observed [$I > 2\sigma(I)$] reflections	7792, 2292, 2228
R_{int}	0.020
$(\sin\theta/\lambda)_{max}$ (Å^{-1})	0.631
Refinement	
$R[F^2 > 2\sigma(F^2)]$, $wR(F^2)$, S	0.018, 0.046, 1.08
No. of reflections	2292
No. of parameters	126
H-atom treatment	H-atom parameters constrained
$\Delta\rho_{max}$, $\Delta\rho_{min}$ (e Å^{-3})	0.35, −0.76

Computer programs: *CrysAlis PRO* (Rigaku Oxford Diffraction, 2015), *SHELXS* (Sheldrick, 2008), *SHELXL2014* (Sheldrick, 2015), *ORTEP-3 for Windows* (Farrugia, 2012), *DIAMOND* (Brandenburg, 2006) and *publCIF* (Westrip, 2010).

References

Aslanov, L. A., Ionov, V. M., Attiya, V. M., Permin, A. B. & Petrosyan, V. S. (1978). *Zh. Strukt. Khim.* **19**, 109–115.

Brandenburg, K. (2006). *DIAMOND*. Crystal Impact GbR, Bonn, Germany.

Contreras, R., Flores-Parra, A., Mijangos, E., Téllez, F., López-Sandoval, H. & Barba-Behrens, N. (2009). *Coord. Chem. Rev.* **253**, 1979–1999.

Dey, D. K., Dasa, M. K. & Nöth, H. (1999). *Z. Naturforsch. Teil B*, **54**, 145–154.

Farrugia, L. J. (2012). *J. Appl. Cryst.* **45**, 849–854.

Groom, C. R., Bruno, I. J., Lightfoot, M. P. & Ward, S. C. (2016). *Acta Cryst.* B**72**, 171–179.

Isaacs, N. W. & Kennard, C. H. L. (1970). *J. Chem. Soc. A*, pp. 1257–1261.

Lee, S. M., Lo, K. M. & Ng, S. W. (2004). *Acta Cryst.* E**60**, m1614–m1616.

McKinnon, J. J., Jayatilaka, D. & Spackman, M. A. (2007). *Chem. Commun.* pp. 3814–3816.

Rigaku Oxford Diffraction (2015). *CrysAlis PRO*. Agilent Technologies Inc., Santa Clara, CA, USA.

Sadiq-ur-Rehman, Saeed, S., Ali, S., Shahzadi, S. & Helliwell, M. (2007). *Acta Cryst.* E**63**, m1788.

Sheldrick, G. M. (2008). *Acta Cryst.* A**64**, 112–122.

Sheldrick, G. M. (2015). *Acta Cryst.* C**71**, 3–8.

Sisido, K., Takeda, Y. & Kinugawa, Z. (1961). *J. Am. Chem. Soc.* **83**, 538–541.

Teoh, S.-G., Yeap, G.-Y., Loh, C.-C., Foong, L.-W., Teo, S.-B. & Fun, H.-K. (1997). *Polyhedron*, **16**, 2213–2221.

Vallet, V., Wahlgren, U. & Grenthe, I. (2003). *J. Am. Chem. Soc.* **125**, 14941–14950.

Wardell, J. L., Jotani, M. M. & Tiekink, E. R. T. (2016). *Acta Cryst.* E**72**, 1618–1627.

Westrip, S. P. (2010). *J. Appl. Cryst.* **43**, 920–925.

Yearwood, B., Parkin, S. & Atwood, D. A. (2002). *Inorg. Chim. Acta*, **333**, 124–131.

supporting information

Acta Cryst. (2017). E**73**, 667-672 [https://doi.org/10.1107/S2056989017005072]

trans-Dichloridobis(dimethyl sulfoxide-κO)bis(4-fluorobenzyl-κC^1)tin(IV): crystal structure and Hirshfeld surface analysis

Nur Adibah Binti Mohd Amin, Rusnah Syahila Duali Hussen, See Mun Lee, Nathan R. Halcovitch, Mukesh M. Jotani and Edward R. T. Tiekink

Computing details

Data collection: *CrysAlis PRO* (Rigaku Oxford Diffraction, 2015); cell refinement: *CrysAlis PRO* (Rigaku Oxford Diffraction, 2015); data reduction: *CrysAlis PRO* (Rigaku Oxford Diffraction, 2015); program(s) used to solve structure: *SHELXS* (Sheldrick, 2008); program(s) used to refine structure: *SHELXL2014* (Sheldrick, 2015); molecular graphics: *ORTEP-3 for Windows* (Farrugia, 2012) and *DIAMOND* (Brandenburg, 2006); software used to prepare material for publication: *publCIF* (Westrip, 2010).

trans-Dichloridobis(dimethyl sulfoxide-κO)bis(4-fluorobenzyl-κC^1)tin(IV)

Crystal data

$[Sn(C_7H_6F)_2Cl_2(C_2H_6OS)_2]$
M_r = 564.08
Monoclinic, $P2_1/c$
a = 8.2363 (1) Å
b = 12.7020 (2) Å
c = 11.4038 (1) Å
β = 110.391 (2)°
V = 1118.28 (3) Å^3
Z = 2
$F(000)$ = 564
D_x = 1.675 Mg m^{-3}
Cu $K\alpha$ radiation, λ = 1.54184 Å
Cell parameters from 6127 reflections
θ = 5.4–76.3°
μ = 13.28 mm^{-1}
T = 100 K
Prism, colourless
0.24 × 0.12 × 0.10 mm

Data collection

Agilent SuperNova, Dual, Cu at zero, AtlasS2 diffractometer
Radiation source: micro-focus sealed X-ray tube, SuperNova (Cu) X-ray Source
Mirror monochromator
ω scans
Absorption correction: multi-scan (CrysAlis PRO; Rigaku Oxford Diffraction, 2015)
T_{min} = 0.636, T_{max} = 1.000
7792 measured reflections
2292 independent reflections
2228 reflections with $I > 2\sigma(I)$
R_{int} = 0.020
θ_{max} = 76.5°, θ_{min} = 5.4°
h = −10→9
k = −15→15
l = −14→14

Refinement

Refinement on F^2
Least-squares matrix: full
$R[F^2 > 2\sigma(F^2)]$ = 0.018
$wR(F^2)$ = 0.046
S = 1.08
2292 reflections
126 parameters
0 restraints
Hydrogen site location: inferred from neighbouring sites
H-atom parameters constrained

$w = 1/[\sigma^2(F_o^2) + (0.0233P)^2 + 0.7527P]$
where $P = (F_o^2 + 2F_c^2)/3$
$(\Delta/\sigma)_{max} < 0.001$

$\Delta\rho_{max} = 0.35$ e Å^{-3}
$\Delta\rho_{min} = -0.76$ e Å^{-3}

Special details

Geometry. All esds (except the esd in the dihedral angle between two l.s. planes) are estimated using the full covariance matrix. The cell esds are taken into account individually in the estimation of esds in distances, angles and torsion angles; correlations between esds in cell parameters are only used when they are defined by crystal symmetry. An approximate (isotropic) treatment of cell esds is used for estimating esds involving l.s. planes.

Fractional atomic coordinates and isotropic or equivalent isotropic displacement parameters (Å²)

	x	*y*	*z*	U_{iso}*/U_{eq}
Sn	0.5000	0.5000	0.5000	0.00673 (6)
Cl1	0.44665 (6)	0.48762 (3)	0.26545 (4)	0.01508 (10)
S1	0.55778 (5)	0.24628 (3)	0.43015 (3)	0.00881 (9)
F1	0.06456 (15)	0.03219 (9)	0.34347 (11)	0.0248 (2)
O1	0.60349 (15)	0.33583 (9)	0.52752 (10)	0.0106 (2)
C1	0.2332 (2)	0.45714 (13)	0.46551 (16)	0.0130 (3)
H1A	0.2054	0.4746	0.5410	0.016*
H1B	0.1583	0.5013	0.3962	0.016*
C2	0.1878 (2)	0.34437 (13)	0.43339 (15)	0.0098 (3)
C3	0.1093 (2)	0.31260 (13)	0.30871 (15)	0.0111 (3)
H3	0.0838	0.3637	0.2440	0.013*
C4	0.0679 (2)	0.20772 (14)	0.27783 (15)	0.0134 (3)
H4	0.0147	0.1868	0.1930	0.016*
C5	0.1058 (2)	0.13487 (13)	0.37280 (16)	0.0140 (3)
C6	0.1822 (2)	0.16192 (14)	0.49747 (16)	0.0144 (3)
H6	0.2062	0.1101	0.5613	0.017*
C7	0.2229 (2)	0.26727 (14)	0.52668 (15)	0.0121 (3)
H7	0.2758	0.2873	0.6118	0.014*
C8	0.6371 (2)	0.13286 (13)	0.52466 (15)	0.0154 (3)
H8A	0.7576	0.1447	0.5786	0.023*
H8B	0.6312	0.0718	0.4708	0.023*
H8C	0.5662	0.1197	0.5766	0.023*
C9	0.7181 (2)	0.25482 (14)	0.35875 (16)	0.0159 (3)
H9A	0.7035	0.3209	0.3118	0.024*
H9B	0.7055	0.1952	0.3017	0.024*
H9C	0.8335	0.2530	0.4235	0.024*

Atomic displacement parameters (Å²)

	U^{11}	U^{22}	U^{33}	U^{12}	U^{13}	U^{23}
Sn	0.00785 (9)	0.00543 (9)	0.00565 (8)	0.00005 (4)	0.00078 (6)	−0.00080 (4)
Cl1	0.0208 (2)	0.0153 (2)	0.00719 (18)	0.00143 (14)	0.00249 (16)	0.00013 (13)
S1	0.00860 (18)	0.00802 (18)	0.00877 (16)	0.00079 (13)	0.00171 (14)	−0.00157 (13)
F1	0.0250 (6)	0.0089 (5)	0.0328 (6)	−0.0026 (4)	0.0006 (5)	−0.0014 (5)
O1	0.0135 (6)	0.0067 (5)	0.0095 (5)	0.0016 (4)	0.0012 (4)	−0.0021 (4)
C1	0.0082 (7)	0.0131 (9)	0.0172 (8)	−0.0007 (6)	0.0039 (6)	−0.0030 (6)

C2	0.0059 (7)	0.0112 (8)	0.0122 (7)	0.0000 (6)	0.0032 (6)	−0.0012 (6)
C3	0.0087 (7)	0.0129 (8)	0.0105 (7)	0.0005 (6)	0.0018 (6)	0.0023 (6)
C4	0.0115 (8)	0.0152 (9)	0.0117 (7)	−0.0004 (6)	0.0020 (6)	−0.0028 (6)
C5	0.0110 (8)	0.0078 (8)	0.0211 (8)	−0.0014 (6)	0.0030 (6)	−0.0018 (6)
C6	0.0117 (8)	0.0151 (8)	0.0152 (8)	0.0015 (6)	0.0032 (6)	0.0065 (6)
C7	0.0089 (8)	0.0176 (8)	0.0090 (7)	−0.0006 (6)	0.0022 (6)	0.0000 (6)
C8	0.0228 (9)	0.0080 (8)	0.0141 (8)	0.0027 (6)	0.0049 (7)	0.0002 (6)
C9	0.0166 (9)	0.0175 (9)	0.0167 (8)	0.0005 (6)	0.0097 (7)	−0.0019 (6)

Geometric parameters (Å, º)

Sn—C1	2.1628 (16)	C3—C4	1.390 (2)
Sn—C1^{i}	2.1628 (16)	C3—H3	0.9500
Sn—O1	2.2332 (11)	C4—C5	1.375 (2)
Sn—O1^{i}	2.2332 (11)	C4—H4	0.9500
Sn—Cl1^{i}	2.5599 (4)	C5—C6	1.383 (2)
Sn—Cl1	2.5599 (4)	C6—C7	1.392 (2)
S1—O1	1.5417 (11)	C6—H6	0.9500
S1—C9	1.7796 (17)	C7—H7	0.9500
S1—C8	1.7815 (17)	C8—H8A	0.9800
F1—C5	1.360 (2)	C8—H8B	0.9800
C1—C2	1.494 (2)	C8—H8C	0.9800
C1—H1A	0.9900	C9—H9A	0.9800
C1—H1B	0.9900	C9—H9B	0.9800
C2—C7	1.400 (2)	C9—H9C	0.9800
C2—C3	1.401 (2)		
C1—Sn—C1^{i}	180.0	C4—C3—C2	121.27 (15)
C1—Sn—O1	95.99 (5)	C4—C3—H3	119.4
C1—Sn—Cl1	90.05 (5)	C2—C3—H3	119.4
C1—Sn—Cl1^{i}	89.95 (5)	C5—C4—C3	118.50 (15)
C1—Sn—O1^{i}	84.01 (5)	C5—C4—H4	120.8
C1—Sn—Cl1^{i}	89.95 (5)	C3—C4—H4	120.8
O1—Sn—Cl1	90.44 (3)	F1—C5—C4	118.88 (15)
O1—Sn—Cl1^{i}	89.56 (3)	F1—C5—C6	118.46 (15)
C1^{i}—Sn—O1	84.01 (5)	C4—C5—C6	122.66 (16)
C1^{i}—Sn—O1^{i}	95.99 (5)	C5—C6—C7	118.07 (15)
O1—Sn—O1^{i}	180.0	C5—C6—H6	121.0
C1^{i}—Sn—Cl1^{i}	90.05 (5)	C7—C6—H6	121.0
O1^{i}—Sn—Cl1^{i}	90.44 (3)	C6—C7—C2	121.47 (15)
O1^{i}—Sn—Cl1	89.56 (3)	C6—C7—H7	119.3
Cl1^{i}—Sn—Cl1	180.000 (18)	C2—C7—H7	119.3
O1—S1—C9	104.51 (8)	S1—C8—H8A	109.5
O1—S1—C8	102.41 (7)	S1—C8—H8B	109.5
C9—S1—C8	98.73 (8)	H8A—C8—H8B	109.5
S1—O1—Sn	127.03 (6)	S1—C8—H8C	109.5
C2—C1—Sn	115.97 (11)	H8A—C8—H8C	109.5
C2—C1—H1A	108.3	H8B—C8—H8C	109.5

Sn—C1—H1A	108.3	S1—C9—H9A	109.5
C2—C1—H1B	108.3	S1—C9—H9B	109.5
Sn—C1—H1B	108.3	H9A—C9—H9B	109.5
H1A—C1—H1B	107.4	S1—C9—H9C	109.5
C7—C2—C3	118.03 (15)	H9A—C9—H9C	109.5
C7—C2—C1	121.12 (14)	H9B—C9—H9C	109.5
C3—C2—C1	120.85 (15)		
C9—S1—O1—Sn	92.64 (10)	C3—C4—C5—F1	179.52 (15)
C8—S1—O1—Sn	−164.80 (9)	C3—C4—C5—C6	0.4 (3)
Sn—C1—C2—C7	81.29 (17)	F1—C5—C6—C7	−179.60 (15)
Sn—C1—C2—C3	−98.42 (16)	C4—C5—C6—C7	−0.5 (3)
C7—C2—C3—C4	−0.3 (2)	C5—C6—C7—C2	0.1 (3)
C1—C2—C3—C4	179.42 (15)	C3—C2—C7—C6	0.2 (2)
C2—C3—C4—C5	0.0 (2)	C1—C2—C7—C6	−179.50 (15)

Symmetry code: (i) −*x*+1, −*y*+1, −*z*+1.

Hydrogen-bond geometry (Å, º)

*Cg*1 is the centroid of the C2–C7 ring.

D—H···*A*	*D*—H	H···*A*	*D*···*A*	*D*—H···*A*
C3—H3···F1^{ii}	0.95	2.49	3.333 (2)	147
C6—H6···Cl1^{iii}	0.95	2.77	3.6129 (18)	148
C8—H8*B*···Cl1^{iv}	0.98	2.76	3.6379 (17)	150
C9—H9*C*···*Cg*1^{v}	0.98	2.67	3.3887 (19)	130

Symmetry codes: (ii) −*x*, *y*+1/2, −*z*+1/2; (iii) *x*, −*y*−1/2, *z*−1/2; (iv) −*x*+1, *y*−1/2, −*z*+1/2; (v) *x*+1, *y*, *z*.